Design Considerations for 2-Level Bearingless Homopolar Motors

Tomislav Strinić[1,2]* Wolfgang Gruber[1,3]† and Fadil Omeragic[1,4]‡

[1] Institute of Electrical Drives and Power Electronics,
Johannes Kepler University Linz
4040 Linz, Austria
[2] `tomislav.strinic@jku.at`
[3] `wolfgang.gruber@jku.at`
[4] `fadil.omeragic@jku.at`

Abstract

The simple rotor structure of 2-level bearingless homopolar motors provides a high mechanical and thermal robustness due to its saliency-based design without permanent magnets. The lack of permanent magnet materials in the rotor significantly reduces costs, but results in lower torque densities. To provide a qualitive overview of viable motor topologies for different stator and rotor pole combinations, this paper provides force and torque performance factors for 2-level bearingless homopolar motors with combined windings. The effects of different tangential displacement angles between the top and the bottom rotor level on the performance factors are investigated and numerically evaluated. Additionally, measurement results of a selected prototype are presented in the bearingless operation.

1 Introduction

Recent developments in the field of electric drives have led to the development of so-called bearingless motors, which are essentially electric motors with magnetic bearings combined into one unit [1]. The magnetic forces for the rotor suspension in such a motor are generated within the motor itself and not in separate magnetic bearings. Nowadays, there is a bearingless counterpart for almost every type of an electric motor [2]. Permanent magnet synchronous machines (PMSM) are widely used for this purpose due to their high power density. Such machines can be designed with either a heteropolar or homopolar permanent magnet air gap field.

The bearingless homopolar motor presented in [3] has an intriguingly simple rotor design, since it is designed as a reluctance rotor without any permanent magnet. This results in a high mechanical and termal robustness. Although the overall cost can be dramatically reduced by eliminating the magnetic material from the rotor, such a design results in lower torque densities.

The motor topology of the bearingless 2-level homopolar reluctance motor introduced in [4] and shown in Figure 1 consists of a stator with a cylindrical permanent magnet in the middle and iron stator teeth, that is, salient poles with concentric coils at each end (top and bottom). The top and bottom teeth arrangement is electrically displaced by 180° for an improved torque generation. This type of a motor can be built either with separate windings in which some phases are dedicated only for force generation, while the remaining phases are used for torque

---

*Performed measurements, processed the data, reviewed the literature, and wrote the manuscript.

†Administrated, supervised, and guided the project, reviewed and edited the manuscript.

‡Designed, optimized, and built the motor, implemented the control, performed measurements, and wrote the digest.
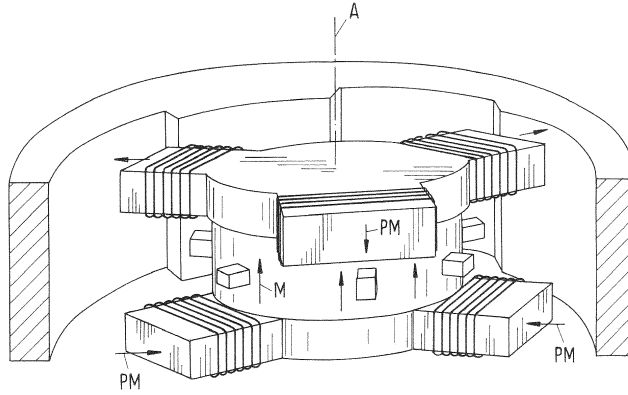
Figure 1: The bearingless 2-level homopolar reluctance motor presented in [4].

generation, or with combined windings in which each phase is used for both force as well as torque generation simultaneously. Combined windings result in reduced losses, but their design and control is more complex [5]. Hence, this paper investigates bearingless 2-level homopolar reluctance motor topologies equipped with combined windings.

Normalized performance factors are used for a qualitative evaluation of torque and force generation based on the force and torque single-phase characteristics introduced in [3]. High performance factor values indicate favorable designs, whereas small values indicate unfavorable designs. This paper therefore presents analytically obtained performance factors calculated for different electrical displacement angles between the top and the bottom rotor teeth of bearingless 2-level homopolar motors that have the top and the bottom stator teeth electrically displaced by 180° relative to each other. The obtained performance factors provide an insight into viable motor topologies for different stator and rotor pole combinations. Additionally, measured force and torque single-phase characteristics of one selected motor design are presented along with measurement results of reference position step responses and disturbance force position responses in the bearingless operation.

2 Mathematical Modeling and Control Scheme

The basis for the analysis, optimization, and control of a bearingless motor is given by its mathematical model. Thus, a sufficiently accurate mathematical description of electro-mechanical relationships is needed for constructing such a model.

2.1 Force and Torque Generation

Among different methods of modeling force and torque generation, methods based on the virtual energy and Maxwell's stress tensor are most frequently used [6]. According to [7], radial forces F_x and F_y that act on the rotor of a magnetically non-saturated electrical machine in the x- and y-direction, respectively, together with the developed torque T_z can generally be obtained from

the rotor position $\mathbf{x}_r = \begin{bmatrix} x_r & y_r & \varphi_r \end{bmatrix}^\mathsf{T}$ and the stator phase currents $\mathbf{i}_s = \begin{bmatrix} i_{s1} & i_{s2} & \ldots & i_{sm} \end{bmatrix}^\mathsf{T}$ as

$$\begin{bmatrix} F_x \\ F_y \\ T_z \end{bmatrix} = \begin{bmatrix} \mathbf{i}_s^\mathsf{T} & \mathbf{0}_{1\times m} & \mathbf{0}_{1\times m} \\ \mathbf{0}_{1\times m} & \mathbf{i}_s^\mathsf{T} & \mathbf{0}_{1\times m} \\ \mathbf{0}_{1\times m} & \mathbf{0}_{1\times m} & \mathbf{i}_s^\mathsf{T} \end{bmatrix} \mathbf{M}_Q(\mathbf{x}_r)\,\mathbf{i}_s + \mathbf{M}_L(\mathbf{x}_r)\,\mathbf{i}_s + \mathbf{M}_C(\mathbf{x}_r). \tag{1}$$

$\mathbf{M}_Q$ in (1) describes the armature reaction and the phase current induced reluctance forces and torques, $\mathbf{M}_L$ describes the interaction between the magnetic field and the stator currents, while $\mathbf{M}_C$ describes the cogging forces and the cogging torque. Moreover, $\mathbf{M}_Q$ is independent of the presence of permanent magnet materials and is typically exploited in reluctance motors and active magnetic bearings, while the term with $\mathbf{M}_L$ is linearly dependent on the stator phase currents and hence refers to Lorentz forces often predominantly responsible for the torque generation in machines with permanent magnets. Additionally, $\mathbf{M}_C$ is only significant for machines with permanent magnets [8].

For small rotor displacements x_r and y_r in the x- and y-direction, respectively, the system can be linearized using Taylor series as

$$\begin{bmatrix} F_x \\ F_y \\ T_z \end{bmatrix} \approx \begin{bmatrix} \mathbf{i}_s^\mathsf{T} & \mathbf{0}_{1\times m} & \mathbf{0}_{1\times m} \\ \mathbf{0}_{1\times m} & \mathbf{i}_s^\mathsf{T} & \mathbf{0}_{1\times m} \\ \mathbf{0}_{1\times m} & \mathbf{0}_{1\times m} & \mathbf{i}_s^\mathsf{T} \end{bmatrix} \mathbf{M}_Q(\varphi_r)\,\mathbf{i}_s + \mathbf{M}_L(\varphi_r)\,\mathbf{i}_s + \mathbf{M}_C(\varphi_r) + \mathbf{K}(\mathbf{i}_s, \varphi_r)\,\mathbf{x}_r, \tag{2}$$

where $\mathbf{x}_r = \begin{bmatrix} x_r & y_r \end{bmatrix}^\mathsf{T}$, while the newly introduced matrix $\mathbf{K}$ is referred to as the stiffness matrix because it describes the negative radial stiffness and consequently the unstable radial behavior of the system. For that reason, a closed control loop is necessary to stabilize the system.

However, in the case of bearingless motors with an air gap field pre-magnetized by permanent magnets, the forces and the torque resulting from $\mathbf{M}_Q$ are often negligible. In such a case, forces and torque can be generated by the stator coils by means of $\mathbf{M}_L$, which is referred to as the current-force matrix and represented by $\mathbf{T}_m(\varphi_r)$ in the unstable rest position $x_r = y_r = 0\,\text{mm}$. Due to the linear dependency of force and torque generation on $\mathbf{i}_s$, superposition of force and torque generating currents is feasible [9].

2.2 Structure of the Current-Force Matrix

For a stator with m phases, $\dim(\mathbf{T}_m(\varphi_r)) = 3 \times m$, whereby $\mathbf{T}_m(\varphi_r)$ can generally be written as

$$\mathbf{T}_m(\varphi_r) = \begin{bmatrix} T_{m,1,1}(\varphi_r) & T_{m,2,1}(\varphi_r) & \cdots & T_{m,m,1}(\varphi_r) \\ T_{m,1,2}(\varphi_r) & T_{m,2,2}(\varphi_r) & \cdots & T_{m,m,2}(\varphi_r) \\ T_{m,1,3}(\varphi_r) & T_{m,2,3}(\varphi_r) & \cdots & T_{m,m,3}(\varphi_r) \end{bmatrix}. \tag{3}$$

In case of symmetrical stator and rotor geometries, the overall $\mathbf{T}_m$ matrix can be calculated from the first column as

$$\begin{bmatrix} T_{m,n,1}(\varphi_r) \\ T_{m,n,2}(\varphi_r) \\ T_{m,n,3}(\varphi_r) \end{bmatrix} = \begin{bmatrix} \cos(\nu) & -\sin(\nu) & 0 \\ \sin(\nu) & \cos(\nu) & 0 \\ 0 & 0 & 1 \end{bmatrix} \begin{bmatrix} T_{m,1,1}(\varphi_r - p_z\nu) \\ T_{m,1,2}(\varphi_r - p_z\nu) \\ T_{m,1,3}(\varphi_r - p_z\nu) \end{bmatrix}, \tag{4}$$

where $\nu = 2\pi(n-1)/m$ for $n \in \mathbb{N}\,|\,1 < n \leq m$ and p_z represents the rotor pole pair number. The first column of $\mathbf{T}_m$ constitutes the force and torque single-phase characteristics. If the x_r direction coincides with the magnetic axis of the first stator coil, then $T_{m,1,1}$ corresponds to F_x, $T_{m,1,2}$ to F_y, and $T_{m,1,3}$ represents T_z generated by that coil. In (4), the nth column of $\mathbf{T}_m$ is

calculated using a rotation matrix to account for the stator fixed force direction and an adapted rotor angle of each phase by assuming the mathematically positive direction of the coil sequence.

The force and torque single-phase characteristics can be determined by means of analytical models, finite element simulations, or measurements. The analytical calculation of $\mathbf{T}_m$ drastically reduces simulation effort, while the only requirement is absence of magnetic saturation, so that the components of $\mathbf{i}_s$ that generate the forces can be superimposed on those that generate the torque [9].

2.3 Control Scheme

The control of a bearingless motor requires properly decoupled components of $\mathbf{i}_s$ responsible for generating F_x, F_y, and T_z. Those components can be obtained from

$$\begin{bmatrix} F_x \\ F_y \\ T_z \end{bmatrix} = \mathbf{T}_m(\varphi_r)\, \mathbf{i}_s, \tag{5}$$

but $\mathbf{T}_m$ needs to be inverted. The inverse of $\mathbf{T}_m$ is denoted by $\mathbf{K}_m$ in terms of which $\mathbf{i}_s$ can be expressed as

$$\mathbf{i}_s = \mathbf{K}_m(\varphi_r) \begin{bmatrix} F_x \\ F_y \\ T_z \end{bmatrix}. \tag{6}$$

According to [7, 10], $\mathbf{K}_m$ for the set of phase currents with minimal resistive power losses can be obtained as

$$\mathbf{K}_m(\varphi_r) = \mathbf{T}_m^{\mathsf{T}}(\varphi_r) \left(\mathbf{T}_m(\varphi_r)\, \mathbf{T}_m^{\mathsf{T}}(\varphi_r) \right)^{-1}, \tag{7}$$

from where it can be seen that $\mathbf{K}_m$ is a Moore-Penrose inverse of $\mathbf{T}_m$ because their product results in an identity matrix. In this way, the reference values of $\mathbf{i}_s$ can be determined based on φ_r for certain reference values of F_x ($F_{x,ref}$), F_y ($F_{y,ref}$), and T_z ($T_{z,ref}$), so that the rotor radial position (x_r and y_r) and the rotor angular speed ω_r can be separately controlled as shown in Figure 2. Hence, $\mathbf{K}_m$ provides the reference values of $\mathbf{i}_s$ used for the calculation of the error terms that are fed into the current controller in the inner control loop. The measured rotor position (x_r and y_r) as well as the measured rotor angle φ_r are used as feedback values to close the outer control loop. Furthermore, x_r and y_r are separately controlled by two independent PID controllers, while ω_r and $\mathbf{i}_s$ are controlled by PI controllers [9].

3 Performance Comparison

From the forces and the torque generated by a single energized stator phase, the overall motor characteristics can be computed for cases when all stator phases are appropriately energized [3]. Based on that notion, performance factors can be defined with respect to the number of rotor poles and stator teeth to provide a way of evaluating different motor topologies.

3.1 Definition of Performance Factors

Performance factors are defined by comparing the forces and the torque generated by a single energized stator phase, which constitute the normalized force and torque single-phase character-istics shown in Figure 3 [9], with those generated by all stator phases appropriately energized
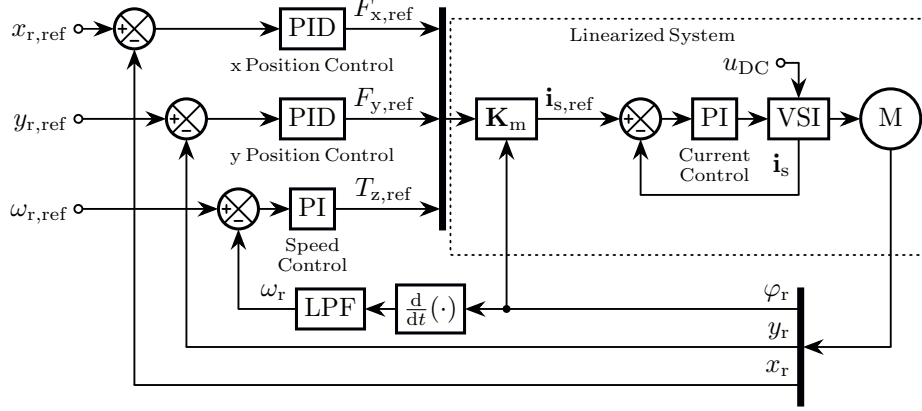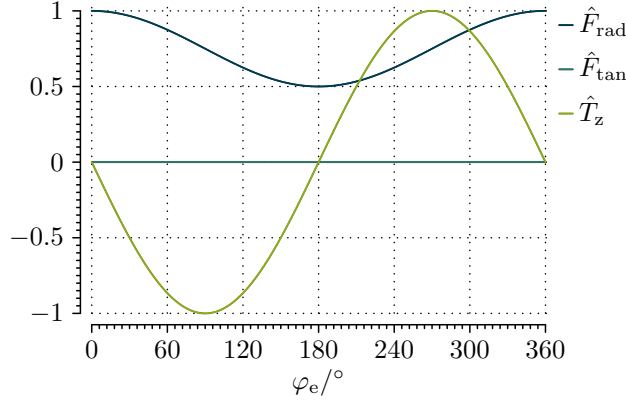
4

Figure 2: A simplified control block diagram.

Figure 3: Normalized force and torque single-phase characteristics.

for the optimal force or torque generation. Those factors are of a great significance, especially for combined coil systems in which the load-bearing forces and the torque are jointly generated by the coils. The performance factors are based on the inverse of $\mathbf{T}_\mathrm{m}$ (that is $\mathbf{K}_\mathrm{m}$) obtained from the force and torque single-phase characteristics. They allow favorable motor topologies with different numbers of rotor and stator teeth to be found without a significant computational effort [7].

The force performance factor c_F describes the ability of a bearingless drive to generate forces and thus provides a comparison value between different machine topologies. It relates the smallest overall force $F_\mathrm{overall,min}$ that can be generated by the motor over the rotor angle to the peak force of a single phase $F_\mathrm{phase,max}$ as

$$c_F = \frac{2}{m_F} \frac{F_\mathrm{overall,min}}{F_\mathrm{phase,max}} = \frac{2}{m_F} \min_{j=1,2} \left(\frac{1}{\max\limits_{i,\varphi_\mathrm{r}} |K_{\mathrm{m},i,j}(\varphi_\mathrm{r})|} \right), \tag{8}$$

where $2/m_F$ represents the normalization factor in which m_F stands for the force-generating stator phases, while $K_{\mathrm{m},i,j}$ represents the entry in the i-th row and j-th column of $\mathbf{K}_\mathrm{m}$ [7, 9, 11].

5

In contrast to the torque generation, in this case an additional degree of freedom must be taken into account. In addition to the rotor rotation angle, the direction of the desired force effect also influences the generation of the load-bearing force. However, the expression for calculation of c_F given by (8) considers only F_x and F_y.

Similarly, the torque performance factor c_T correlates the smallest overall torque $T_{\text{overall,min}}$ that the motor can generate over the rotor angle with the peak torque of a single phase $T_{\text{phase,max}}$ as

$$c_T = \frac{2}{m_T} \frac{T_{\text{overall,min}}}{T_{\text{phase,max}}} = \frac{2}{m_T} \frac{1}{\max\limits_{i,\varphi_r} |K_{\text{m},i,3}(\varphi_r)|},\tag{9}$$

where $2/m_T$ represents the normalization factor in which m_T stands for the torque-generating stator phases [7, 9].

3.2 Force and Torque Performance Factors for 2-Level Bearingless Homopolar Motors

Force and torque performance factors of a 2-level homopolar motor can be determined from the normalized force and torque single-phase characteristics shown in Figure 3, which represent first harmonic approximations. It can be seen that the normalized radial force $\hat{F}_{\text{rad}}$ is a cosine function of the electrical angle φ_e ($\varphi_e = p_z \varphi_r$) with an offset, whereas the normalized tangential force $\hat{F}_{\text{tan}}$ is zero, while the normalized motor torque $\hat{T}_z$ is a negative sine function of φ_e.

In contrast to the performance factors presented in [9], a stator with two levels is examined here. Additionally, the top and the bottom stator teeth are electrically displaced by 180°. The calculated force and torque performance factors listed in Table 1, Table 2, and Table 3 are calculated for the top and the bottom rotor teeth electrically displaced by 0°, 90°, and 180°, respectively, and provide an overview of viable motor topologies. The combinations of high performance factors reveals favorable topologies, whereas low performance factors indicate unfavorable designs. All combinations with $p_z = m$ can be excluded due to high cogging torques. In the observed case the choice of the motor topology is limited by the requirement of the motor to have six phases ($m = 6$) per each level. Thus, based on the required number of phases and according to the performance factors given in the presented tables, a combination with either eight ($p_z = 8$) or ten rotor teeth ($p_z = 10$) for six phases per each level is sensible. Since ten rotor teeth result in a higher electrical frequency than eight rotor teeth and a more powerful processor is therefore necessary for control, the rotor tooth number was chosen to be eight due to the good average motor characteristics in all three presented cases shown in Tables 1–3.
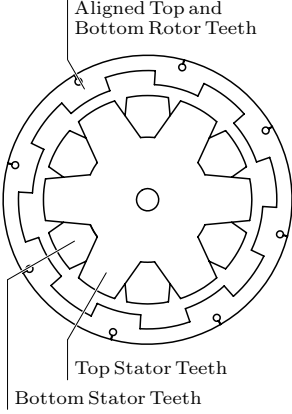
4 Prototype and Measurements

Although the following measurements were performed with tangentially aligned top and bottom rotor teeth, the rotor was built in a way to enable displacement of the top and the bottom rotor teeth as it can be seen in Figure 4.
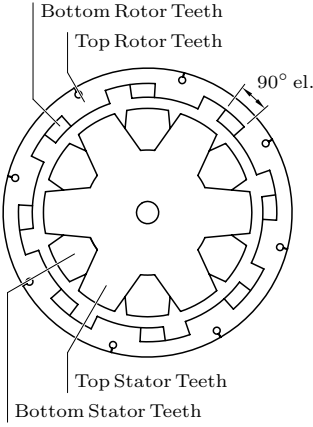
4.1 Static Measurements

To verify the theoretical proposition of the force and torque single-phase characteristics, a static measurement was performed first by supplying a constant current linkage of 616 A-turns to a single stator phase of the bottom level of the motor. The resulting characteristics of the

	$m = 4$	$m = 5$	$m = 6$	$m = 7$	$m = 8$
$p_z = 4$	$c_F = 0.6$	$c_F = 0.6$	$c_F = 0.6$	$c_F = 0.6$	$c_F = 0.6$
	$c_T = 0$	$c_T = 1$	$c_T = 0.9$	$c_T = 1$	$c_T = 1$
$p_z = 5$	$c_F = 0.6$	$c_F = 0.6$	$c_F = 0.6$	$c_F = 0.6$	$c_F = 0.7$
	$c_T = 1$	$c_T = 0$	$c_T = 1$	$c_T = 1$	$c_T = 1$
$p_z = 6$	$c_F = 0.7$	$c_F = 0.6$	$c_F = 0.6$	$c_F = 0.6$	$c_F = 0.6$
	$c_T = 1$	$c_T = 1$	$c_T = 0$	$c_T = 1$	$c_T = 1$
$p_z = 7$	$c_F = 0$	$c_F = 0.6$	$c_F = 0.6$	$c_F = 0.6$	$c_F = 0.6$
	$c_T = 0.1$	$c_T = 1$	$c_T = 1$	$c_T = 0$	$c_T = 1$
$p_z = 8$	$c_F = 0.5$	$c_F = 0.7$	$c_F = 0.6$	$c_F = 0.6$	$c_F = 0.6$
	$c_T = 0$	$c_T = 1$	$c_T = 0.9$	$c_T = 1$	$c_T = 0$
$p_z = 9$	$c_F = 0$	$c_F = 0.1$	$c_F = 0.6$	$c_F = 0.6$	$c_F = 0.6$
	$c_T = 0.1$	$c_T = 0.1$	$c_T = 1$	$c_T = 1$	$c_T = 1$
$p_z = 10$	$c_F = 0.7$	$c_F = 0.5$	$c_F = 0.7$	$c_F = 0.6$	$c_F = 0.5$
	$c_T = 1$	$c_T = 0$	$c_T = 1$	$c_T = 1$	$c_T = 0$
$p_z = 11$	$c_F = 0.6$	$c_F = 0.1$	$c_F = 0.1$	$c_F = 0.6$	$c_F = 0.6$
	$c_T = 1$	$c_T = 0.1$	$c_T = 0.1$	$c_T = 0.9$	$c_T = 1$
$p_z = 12$	$c_F = 0.6$	$c_F = 0.7$	$c_F = 0.5$	$c_F = 0.7$	$c_F = 0.6$
	$c_T = 0$	$c_T = 1$	$c_T = 0$	$c_T = 1$	$c_T = 1$

Table 1: Performance factors for the top and bottom rotor teeth electrically displaced by 0°.

	$m = 4$	$m = 5$	$m = 6$	$m = 7$	$m = 8$
$p_z = 4$	$c_F = 0.5$	$c_F = 0.4$	$c_F = 0.6$	$c_F = 0.6$	$c_F = 0.6$
	$c_T = 1$	$c_T = 0.6$	$c_T = 1$	$c_T = 0.9$	$c_T = 0.1$
$p_z = 5$	$c_F = 0.4$	$c_F = 0.6$	$c_F = 0.4$	$c_F = 0.6$	$c_F = 0.6$
	$c_T = 0.7$	$c_T = 1$	$c_T = 0.7$	$c_T = 1$	$c_T = 1$
$p_z = 6$	$c_F = 0.7$	$c_F = 0.4$	$c_F = 0.5$	$c_F = 0.4$	$c_F = 0.6$
	$c_T = 0.1$	$c_T = 0.6$	$c_T = 1$	$c_T = 0.7$	$c_T = 1$
$p_z = 7$	$c_F = 0.4$	$c_F = 0.6$	$c_F = 0.4$	$c_F = 0.5$	$c_F = 0.4$
	$c_T = 0.6$	$c_T = 0.9$	$c_T = 0.7$	$c_T = 1$	$c_T = 0.7$
$p_z = 8$	$c_F = 0.5$	$c_F = 0.6$	$c_F = 0.6$	$c_F = 0.4$	$c_F = 0.5$
	$c_T = 1$	$c_T = 1$	$c_T = 1$	$c_T = 0.7$	$c_T = 1$
$p_z = 9$	$c_F = 0.4$	$c_F = 0.4$	$c_F = 0.6$	$c_F = 0.6$	$c_F = 0.4$
	$c_T = 0.7$	$c_T = 0.6$	$c_T = 0.1$	$c_T = 1$	$c_T = 0.7$
$p_z = 10$	$c_F = 0.7$	$c_F = 0.5$	$c_F = 0.6$	$c_F = 0.6$	$c_F = 0.6$
	$c_T = 0.1$	$c_T = 1$	$c_T = 0.9$	$c_T = 1$	$c_T = 1$
$p_z = 11$	$c_F = 0.4$	$c_F = 0.4$	$c_F = 0.4$	$c_F = 0.6$	$c_F = 0.6$
	$c_T = 0.7$	$c_T = 0.7$	$c_T = 0.7$	$c_T = 0.9$	$c_T = 1$
$p_z = 12$	$c_F = 0.5$	$c_F = 0.6$	$c_F = 0.5$	$c_F = 0.6$	$c_F = 0.6$
	$c_T = 1$	$c_T = 1$	$c_T = 1$	$c_T = 1$	$c_T = 0.1$

Table 2: Performance factors for the top and bottom rotor teeth electrically displaced by 90°.

	$m = 4$	$m = 5$	$m = 6$	$m = 7$	$m = 8$
$p_{\mathrm{z}} = 4$	$c_F = 0.6$	$c_F = 0.6$	$c_F = 0.6$	$c_F = 0.6$	$c_F = 0.6$
	$c_T = 1$	$c_T = 1$	$c_T = 0.9$	$c_T = 1$	$c_T = 1$
$p_{\mathrm{z}} = 5$	$c_F = 0.6$	$c_F = 0.6$	$c_F = 0.6$	$c_F = 0.6$	$c_F = 0.6$
	$c_T = 1$	$c_T = 0$	$c_T = 1$	$c_T = 1$	$c_T = 1$
$p_{\mathrm{z}} = 6$	$c_F = 0.7$	$c_F = 0.6$	$c_F = 0.6$	$c_F = 0.6$	$c_F = 0.6$
	$c_T = 1$	$c_T = 1$	$c_T = 0.1$	$c_T = 1$	$c_T = 1$
$p_{\mathrm{z}} = 7$	$c_F = 0$	$c_F = 0.6$	$c_F = 0.6$	$c_F = 0.6$	$c_F = 0.6$
	$c_T = 0.1$	$c_T = 1$	$c_T = 1$	$c_T = 0.1$	$c_T = 1$
$p_{\mathrm{z}} = 8$	$c_F = 0.5$	$c_F = 0.7$	$c_F = 0.6$	$c_F = 0.6$	$c_F = 0.6$
	$c_T = 0$	$c_T = 1$	$c_T = 0.9$	$c_T = 1$	$c_T = 0$
$p_{\mathrm{z}} = 9$	$c_F = 0$	$c_F = 0.1$	$c_F = 0.6$	$c_F = 0.6$	$c_F = 0.6$
	$c_T = 0.1$	$c_T = 0.1$	$c_T = 1$	$c_T = 1$	$c_T = 1$
$p_{\mathrm{z}} = 10$	$c_F = 0.7$	$c_F = 0.5$	$c_F = 0.7$	$c_F = 0.6$	$c_F = 0.6$
	$c_T = 1$	$c_T = 0$	$c_T = 1$	$c_T = 1$	$c_T = 1$
$p_{\mathrm{z}} = 11$	$c_F = 0.6$	$c_F = 0.1$	$c_F = 0.1$	$c_F = 0.6$	$c_F = 0.6$
	$c_T = 1$	$c_T = 0.1$	$c_T = 0.1$	$c_T = 0.9$	$c_T = 1$
$p_{\mathrm{z}} = 12$	$c_F = 0.6$	$c_F = 0.7$	$c_F = 0.5$	$c_F = 0.7$	$c_F = 0.6$
	$c_T = 0$	$c_T = 1$	$c_T = 0$	$c_T = 1$	$c_T = 1$

Bottom Rotor Teeth
Top Rotor Teeth
180° el.
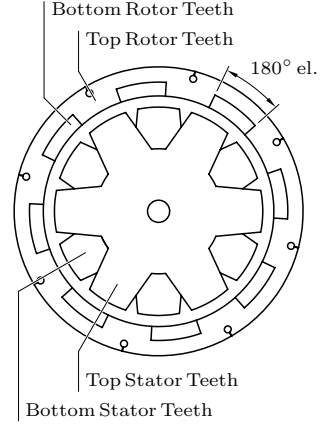Top Stator Teeth
Bottom Stator Teeth

Table 3: Performance factors for the top and bottom rotor teeth electrically displaced by 180°.
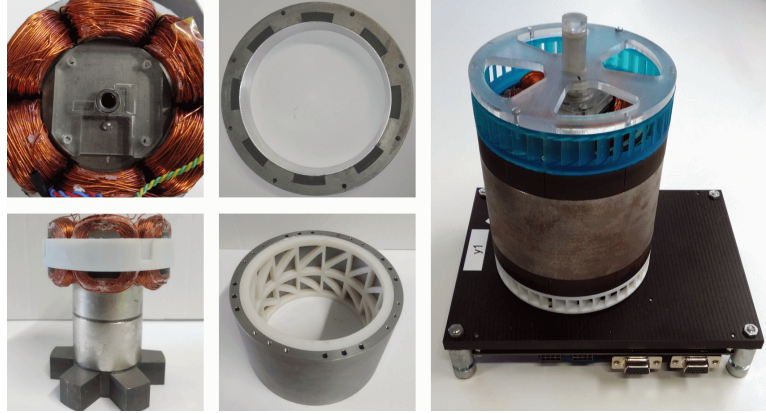

Figure 4: The top stator windings (top left), the stator with the top windings (bottom left), the laminated rotor teeth with the pressed-in aluminum ring (top center), the rotor center piece (bottom center), and the final motor setup (right).

radial force F_{rad} and the tangential force F_{tan} shown with the characteristic of the torque T_{z} in Figure 5, aside from not being normalized, closely match the corresponding waveforms presented in Figure 3. Since oscillations in F_{tan}, which is perpendicular to the magnetic axis of the energized stator coil, is expected to be less than 10% of F_{rad}, F_{tan} in Figure 3 is taken as zero [3]. Based on the maximum value of F_{rad} in Figure 5, which corresponds to $F_{\mathrm{phase,max}}$ in
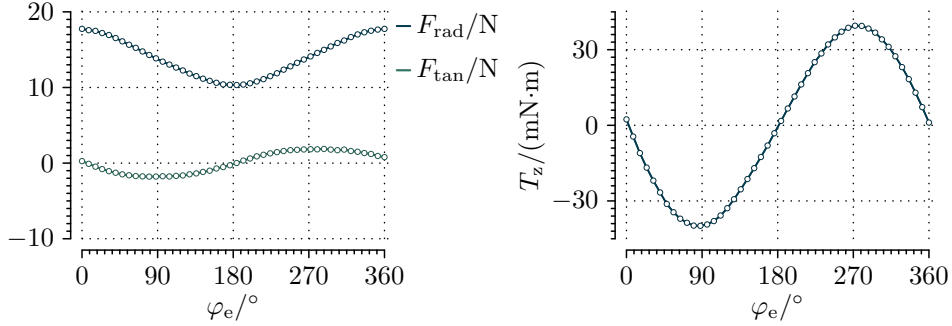
Figure 5: Measured force (left) and torque (right) single-phase characteristics.

(8), and the force performance factor highlighted in Table 1, $F_{\text{overall,min}}$ can be obtained as

$$F_{\text{overall,min}} = \frac{c_F m_F}{2} F_{\text{phase,max}}. \tag{10}$$

Similarly, $T_{\text{overall,min}}$ can be obtained based on the torque performance factor highlighted in Table 1 and the peak value of T_z, which corresponds to $T_{\text{phase,max}}$ in (9), as

$$T_{\text{overall,min}} = \frac{c_T m_T}{2} T_{\text{phase,max}}. \tag{11}$$

In both (10) and (11), $m_F = m_T = 12$ because the presented motor has twelve combined windings, that is, six windings on each level.

4.2 Measurements in the Bearingless Operation

Due to the unstable behavior of the rotor in the radial direction, active position and speed control are necessary for the operation as a bearingless drive. The control was implemented with a six-phase voltage source inverter (VSI) that has a DC-Link voltage of 350 V and delivers a maximum effective output phase current of 10 A. Since it has six half-bridges and the motor has twelve coils, two such inverters were required, one for the top and one for the bottom level. The control was designed under MATLAB® Simulink® [12] with X2C [13] rapid prototyping tool for code generation of real-time control algorithms for microprocessors. Since the motor is composed of two levels, the measurements for each level were carried out at a standstill but in the levitating state.

4.2.1 Reference Position Step Responses

To test the position control in both the x- and the y-direction, a step in the reference position of the rotor in the x-direction $x_{\text{r,ref}}$ from 0 mm to 0.05 mm was performed first, while keeping the reference position of the rotor in the y-direction $y_{\text{r,ref}}$ at 0 mm. Next, a step in $y_{\text{r,ref}}$ from 0 mm to 0.05 mm was performed, while keeping $x_{\text{r,ref}}$ at 0 mm. This procedure was done for each level of the motor and the results are shown in Figure 6, where the longer settling time of the top level is a result of lower dynamics of the PID controllers. In the observed case, 0 mm position in either direction represents the radially centered position of the rotor with respect to the stator, where the maximum radial displacement in any direction corresponds to the air gap and amounts to 0.5 mm. It can also be seen that a practically full decoupling of the x- and the y-direction can be achieved with the proposed control system shown in Figure 2.
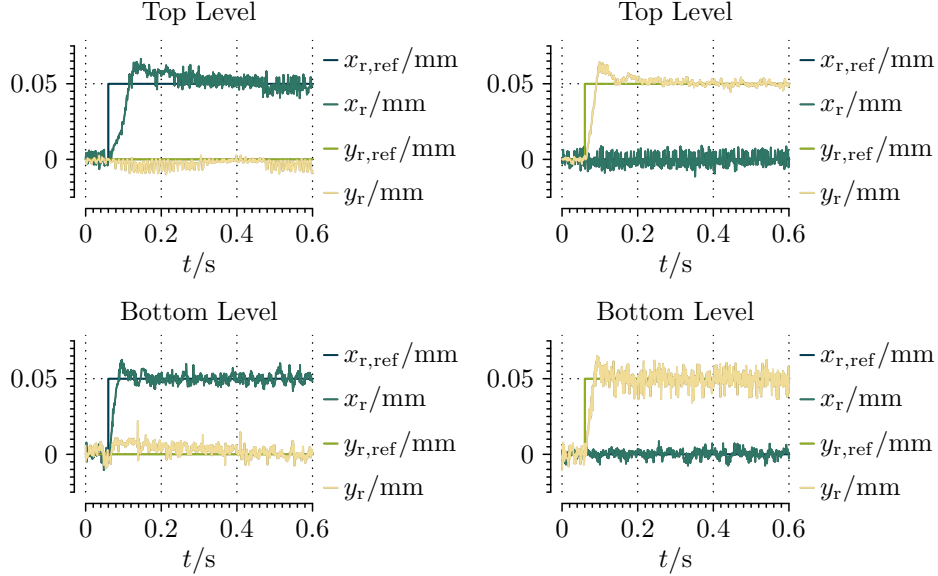
9

Figure 6: Reference position step responses.

4.2.2 Disturbance Force Position Responses

In order to examine the interference suppression capabilities of the position control, both $x_{\mathrm{r,ref}}$ and $y_{\mathrm{r,ref}}$ were kept at $0\,\mathrm{mm}$ and a step disturbance force with the magnitude of $3\,\mathrm{N}$ was first applied in the x- and then in the y-direction. The results are presented in Figure 7 for both the top and the bottom level. From those results it can be seen that although the rotor initially moves out of the center position in the direction of the disturbance force, the controllers quickly manage to compensate the disturbance so that the rotor returns back to the center.

5 Conclusion

This paper has presented normalized performance factors that provide a useful way of gaining an insight into the torque and radial force generation of 2-level bearingless homopolar motors [3]. The analytically obtained performance factors listed in Tables 1–3 are calculated for three different electrical displacement angles between the top and the bottom rotor teeth, with the top and the bottom stator teeth electrically displaced by 180°.

An optimal motor design was selected based on a combination of performance factors while taking into account the requirement of the motor to have six phases per each level and avoiding combinations in which the number of stator phases is equal to the number of the rotor pole pairs due to high cogging torques. Although the rotor of the presented motor was mechanically designed to enable electrical displacement of the top and the bottom rotor teeth by 0°, 90°, and 180°, the measurement results are presented for aligned top and bottom rotor teeth.

The characteristics of the measured force and torque single-phase characteristics presented in Figure 5 closely resembles the theoretical characteristics shown in Figure 3 and thus can be used for calculating the minimum overall force and torque as well as for generating the current-force matrix ($\mathbf{T}_{\mathrm{m}}$) and consequently its inverse ($\mathbf{K}_{\mathrm{m}}$) used in the control scheme of the motor. The
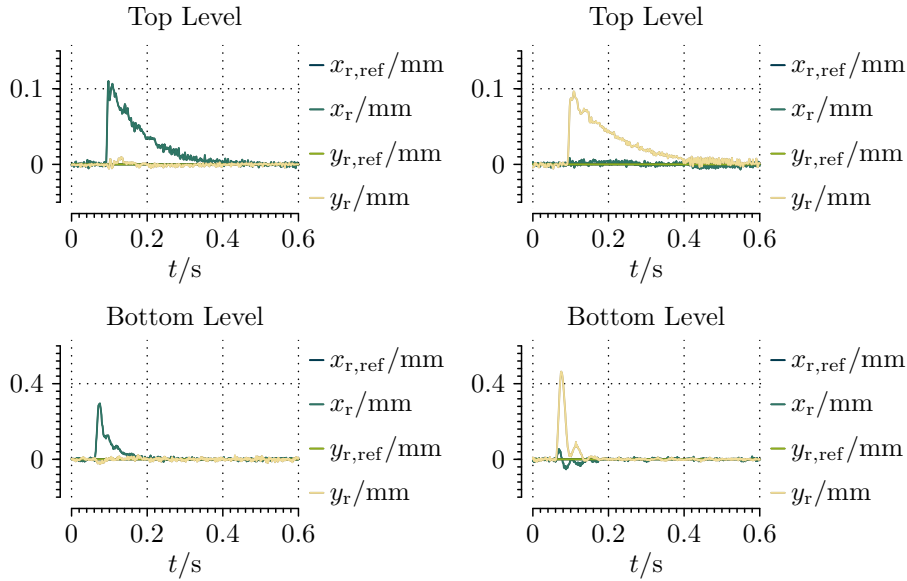
Figure 7: Disturbance force position responses.

measurement results of reference position step responses, disturbance force position responses in the bearingless operation show that a practically fully decoupled control of the x- and the y-direction is achieved with the linearization of the system shown in Figure 2.

6   Acknowledgments

References

[1] J. Bichsel, "The bearingless electrical machine," in *Proc. of the International Symposium on Magnetic Suspension Technology (ISMST)*.   NASA, Langley Research Center: NASA Conference Publication 3152, 1992, pp. 561–574.

[2] A. Chiba, T. Fukao, O. Ichikawa, M. Oshima, M. Takemoto, and D. Dorrell, *Magnetic Bearings and Bearingless Drives*.   Elsevier Ltd, 2005.

[3] W. Gruber, M. Rothböck, and R. T. Schöb, "Design of a novel homopolar bearingless slice motor with reluctance rotor," *IEEE Transactions on Industry Applications*, vol. 51, no. 2, pp. 1456–1464, 2015, DOI: 10.1109/TIA.2014.2341739.

[4] R. Schöb, J. Hugel, and T. Holenstein, "Electromagnetic rotary drive," February 2017. [Online]. Available: https://patents.google.com/patent/EP3115616A1/en

[5] R. Klaus, J. W. Kolar, and T. Nussbaumer, "Comparison of winding concepts for bearingless pumps," in *Proc. of the 7th International Conference on Power Electronics (ICPE)*, 2007, pp. 1013–1020, DOI: 10.1109/ICPE.2007.4692535.

[6] D. J. Griffiths, *Introduction to Electrodynamics (3rd Edition)*.   Pearson Benjamin Cummings, 2008.

[7] H. Grabner, W. Amrhein, S. Silber, and W. Gruber, "Nonlinear feedback control of a bearingless brushless dc motor," *IEEE/ASME Transactions on Mechatronics*, vol. 15, no. 1, pp. 40–47, 2010, DOI: 10.1109/TMECH.2009.2014058.

[8] W. Gruber, W. Amrhein, S. Silber, H. Grabner, and M. Reisinger, "Theoretical analysis of force and torque calculation in magnetic bearing systems with circular airgap," in *Proc. of the 8th International Symposium on Magnetic Suspension Technology (ISMST8)*, Dresden, Germany, 2005, pp. 167–171.

[9] W. Gruber, *Bearingless Slice Motor Systems without Permanent Magnetic Rotors*.   TRAUNER Verlag + Buchservice GmbH, 2017.

[10] H. Grabner, S. Silber, and W. Amrhein, "Bearingless torque motor – modeling and control," in *Proc. of 13th International Symposium on Magnetic Bearings 2012 (ISMB13)*, Arlington, Virginia, USA, 2012, pp. 1–13.

[11] W. Gruber, W. Briewasser, M. Rothböck, and R. T. Schöb, "Bearingless slice motor concepts without permanent magnets in the rotor," in *Proc. of the 2013 IEEE International Conference on Industrial Technology (ICIT)*, Cape Town, South Africa, 2013, pp. 259–265.

[12] The MathWorks Inc., "MATLAB® Simulink®." [Online]. Available: https://www.mathworks.com/products/simulink.html

[13] Linz Center of Mechatronics GmbH, "X2C." [Online]. Available: https://x2c.lcm.at/